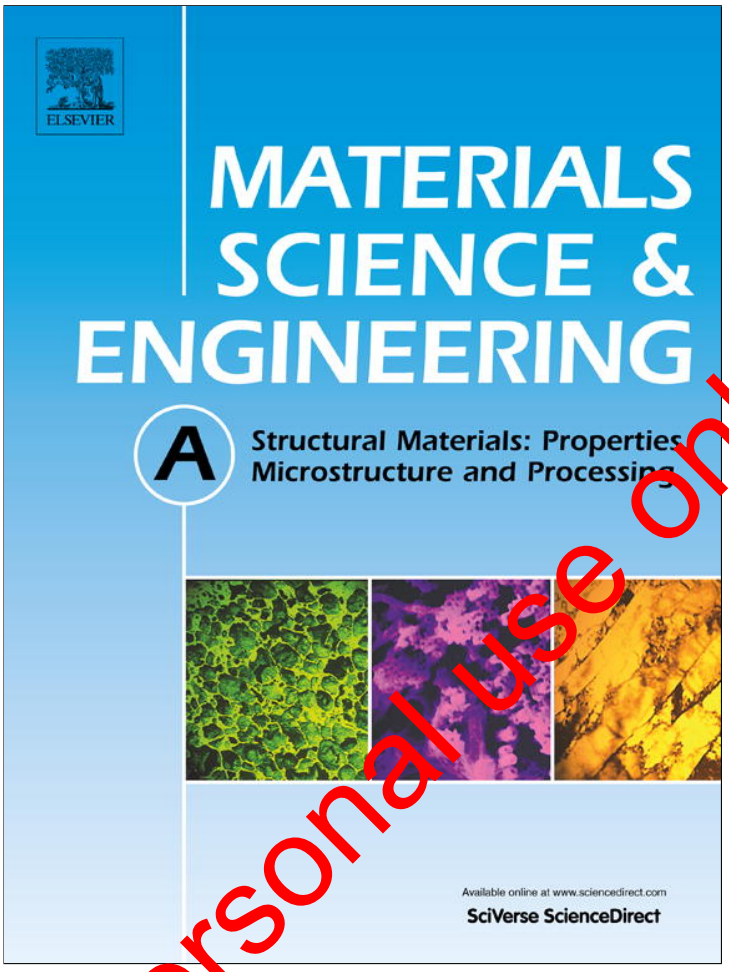

(This is a sample cover image for this issue. The actual cover is not yet available at this time.)

Materials Science & Engineering A 570 (2013) 92–101

Contents lists available at SciVerse ScienceDirect

Materials Science & Engineering A

journal homepage: www.elsevier.com/locate/msea

Influence of high temperature deformation and double tempering on the microstructure of a H21 tool steel

M. Nurbanasari [a,b,*], P. Tsakiropoulos [a], E.J. Palmiere [a]

[a] Department of Materials Science and Engineering, The University of Sheffield, Sheffield S1 3JD, United Kingdom
[b] Department of Mechanical Engineering, Institut Teknologi Nasional, Bandung, Indonesia

ARTICLE INFO

Article history:
Received 22 August 2012
Received in revised form
26 January 2013
Accepted 29 January 2013
Available online 8 February 2013

Keywords:
Thermomechanical processing
Precipitation
Dislocations
Electron microscopy

ABSTRACT

An axisymmetric compression test was used to study the effect of hot deformation and double tempering on the microstructure and hardness of a H21 tool steel. The compression tests used a constant true strain rate of 0.01 s^{-1}, and were performed in the temperature range 1000–1100 °C after austenising at temperatures of either 1100 or 1250 °C. The double tempering was carried out at 650, 750 and 800 °C, with air cooling in between the first and second temper. An overview of the flow curves and the characterisation of microstructures showed no evidence of dynamic recrystallisation. The increase in flow stress with decreasing austenising and deformation temperature was attributed to dislocation movement and the presence of fine and dispersed carbides causing a Zener pinning effect. Without double tempering, the highest hardness was measured after austenising at 1250 °C, followed by deformation at 1000 °C and water quenching (617 HV). No secondary hardening phenomena occurred after double tempering for samples that were first subjected to hot deformation, and the highest double tempered hardness (354 HV) occurred after a double temper at 650 °C following an austenising temperature of 1250 °C and subsequent deformation at temperature of 1000 °C.

1. Introduction

The H21 tungsten hot work tool steel is widely used for high working temperature applications, such as die-casting dies and forging dies due to its resistance to deformation at elevated temperature, high hot hardness, and high compressive strength [1]. This tool steel contains a high concentration of carbide forming elements that tends to promote segregation and form brittle eutectic carbide networks, which consequently decreases the toughness [2]. The H21 tool steels are usually used in the heat treated condition. This heat treatment involves austenising to dissolve the carbides, followed by oil quenching which transforms the austenite to martensite. Finally, these steels are tempered to produce a secondary hardening effect, which provides high strength at both ambient and elevated temperatures. Previous work [3,4] has reported that it is difficult to dissolve the carbides during the austenising process due to the thermodynamic stability of the carbides. Thus, the carbide networks are still present after austenisation, and as a consequence, the hot workability of the tool steel is reduced.

Earlier investigations [5–7] reported that the controlled thermomechanical processing (TMP) is an effective method to control the microstructure, break up the carbide network and optimise the mechanical properties owing to refinement of the carbides and their uniform distribution. Furthermore, through TMP, the austenite grain size will be refined as a result of strain accumulation producing a higher density of nucleation sites and consequently refinement of final microstructure, as reported in [8–10]. However, the carbide forming elements in the tool steels present problems to hot deformation in terms of a narrow hot working temperature range [11]. The lower limit is defined by the type, size and morphology of carbides located along the grain boundaries and within grain interiors. The upper limit is determined by the incipient melting of eutectic carbides and by segregation of low melting point phases along the grain boundaries [4,12]. Though the studies on tool steels are extensive [4,13–17], the study of the effect of combining TMP and a double tempering process on the H21 tool steel is still limited. In this paper, microstructural evolution and variation of hardness during hot deformation and double tempering of a H21 tool steel were investigated. The precipitation behaviour was also studied. It is intended that this information will add to the existing knowledge base regarding the choice of appropriate hot deformation and heat treatment parameters to achieve desired microstructure and properties.

* Corresponding author at: Department of Materials Science and Engineering, The University of Sheffield, Sheffield, S1 3JD, United Kingdom.
Tel.: +44 114 222 5941; fax: +44 114 222 5943.
E-mail addresses: mtq09mn@sheffield.ac.uk, nurbanasarimeilinda@yahoo.com (M. Nurbanasari), p.tsakiropoulos@sheffield.ac.uk (P. Tsakiropoulos), e.j.palmiere@sheffield.ac.uk (E.J. Palmiere).

0921-5093/$ - see front matter © 2013 Elsevier B.V. All rights reserved.
http://dx.doi.org/10.1016/j.msea.2013.01.067

2. Experimental procedure

The chemical composition (wt%) of the investigated H21 tool steel is shown in Table 1. This tool steel was melted at 1590 °C using a vacuum induction laboratory furnace with air cooling to produce an ingot of square cross-section with size $28.5 \times 7 \times 6.5$ cm^3. The high temperature axisymmetric compression tests were carried out on a SERVOTEST thermomechanical compression (TMC) machine. The samples were 12 mm in diameter and 15 mm in height and had thermocouple holes of 1.1 mm in diameter in the middle and 5 mm depth. The schedule for the investigation process is shown in Fig. 1.

The samples were heated up to the respective austenising temperatures at a rate of 15 °C/s and were held at the temperature for 10 min for equilibration. The samples were then cooled to the respective deformation temperatures at a rate of 2 °C/s, held for 10 min, and then deformed to a true equivalent strain of 0.5 at a constant true strain rate of 0.01 s^{-1} followed by water quenching. The deformation tests were done at three different temperatures, namely 1000, 1050 and 1100 °C with austenising temperatures of 1100 and 1250 °C. The deformed samples were cut along the longitudinal compression axis and prepared for the double tempering process, and optical and scanning electron microscopy (SEM) using the standard metallography procedures. The double tempering process was carried out with three different tempering temperatures, namely 650, 750 and 800 °C [1] with air cooling in between the first and second tempering stages. The SEM studies were conducted on a JEOL 6400 equipped with EDS and an INCA software and operated at 20 kV, and an Inspect F microscope. For additional confirmation of the types of carbides, X-ray diffraction of bulk specimens was performed using cobalt radiation. The specimens were scanned in the 2θ angle range 30–130° with a step size of 0.02° and a counting time 1°/min. Thin foils of some deformed samples were prepared for TEM studies using a standard electrolytic jet polishing method. The TEM work was performed on a Philips 420 microscope operated at 120 kV and a JEOL 2010F operated at 200 kV. The hardness was measured using a CV Instrument Vickers hardness tester (model 430 AAT) with load 10 kg and dwell time 15 s. The average diameter of the carbides was measured without differentiation or type by type using an ImageJ software. More than 1500 carbides for each condition were quantified.

Table 1
Chemical composition of the investigated tool steel (wt%).

Tool steel	C	Si	Mn	P	S	Cr	Mo	Ni	W	V	Co
H21	0.3	0.3	0.3	0.03	0.02	3.1	< 0.02	0.3	7.5	0.4	< 0.02

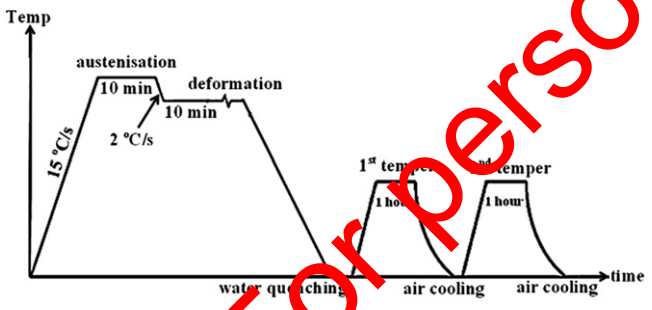

Fig. 1. Schematic diagram of high axisymmetric compression and double tempering process.

3. Results and discussion

3.1. As cast structure

The microstructure of the as cast H21 tool steel consisted of ferrite and carbides, which was predominantly located along the grain boundaries.

The back scattered electron SEM images showed only one type of carbide that appeared as white particles with rodlike, spherical and irregular morphologies, Fig. 2. These carbides were identified by SEM–EDS as M_6C carbides with the typical EDS spectrum in Fig. 2 showing the high W and Fe peaks and with W content four times that of Cr. Quantitative SEM–EDS of the M_6C carbides gave 4% V, 4.2% Cr, 16.6% W and 78.8% Fe (wt%). Fine carbides were identified by TEM as MC carbides having diameters between 5 and 10 nm (Fig. 3). The presence of ferrite and M_6C carbides was also confirmed by XRD (Fig. 4).

The peak positions of the ferrite agreed well with the ICDD card numbers 3-411 and 54-331 and the peak positions for the M_6C (Fe_3W_3C) carbides were in good agreement with the ICDD card number 41-1351. Thus, the Fe_3W_3C carbide was the main primary carbide in the tool steel. The as-cast hardness was 483 ± 6 HV.

3.2. Flow stress

Fig. 5 shows the flow curves of the H21 tool steel after hot deformation at 1000, 1050 and 1100 °C following different austenising temperatures. The Q_{def} value was not calculated because this study only focused on one strain rate (0.01 s^{-1}). To get an

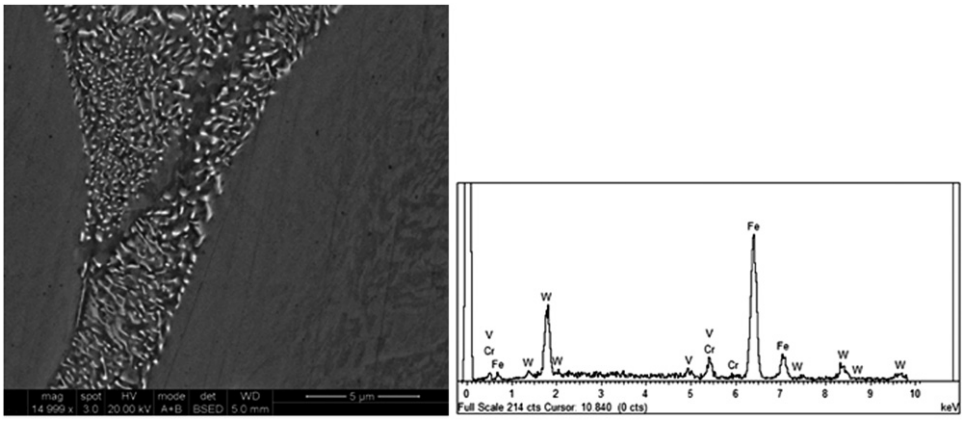

Fig. 2. Back scattered SEM image and EDS spectrum of M_6C carbides of as cast H21 tool steel.

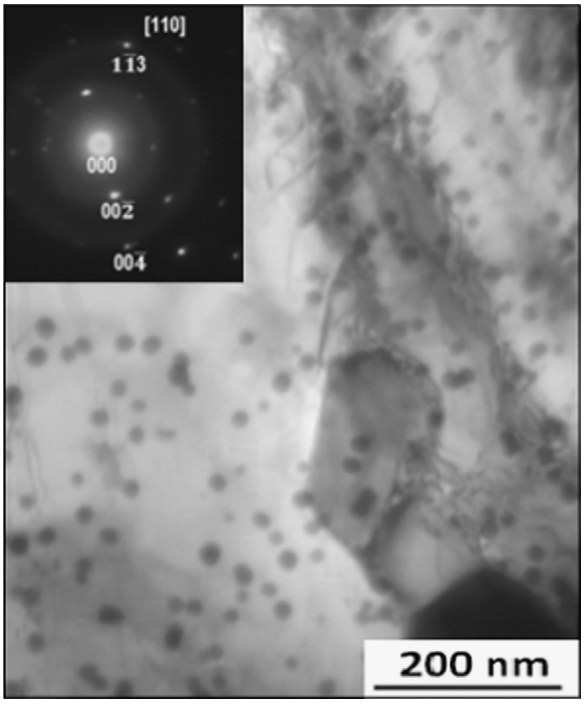

Fig. 3. Bright field TEM image showing the fine dispersed spherical MC carbides of the as cast H21 tool steel and selected area diffraction pattern of a MC carbide.

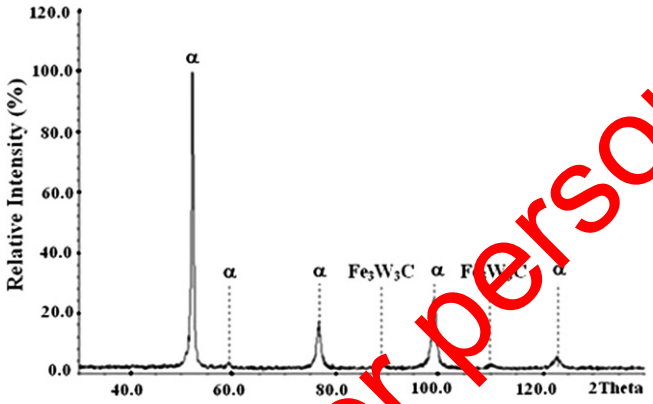

Fig. 4. X-ray diffractogram of the as cast H21 tool steel.

overview of the flow curve behaviour, and to correct the effects of deformational heating, the flow stress was calculated using Q_{def} (607 kJ/mol) that was taken from the literature [18], taking into account hot working with a similar strain rate, chemical composition of steel and volume fraction of carbides.

The shapes of all flow curves were almost identical, i.e., fluctuation features and no peak in flow curves which are indicative of no dynamic recrystallisation having occurred. It can be seen clearly in Fig. 5 that the flow stress increased with decreasing austenising and deformation temperatures. This indicated that the temperature had a significant effect on the flow stress, which has been attributed to dislocation movement [19,20]. The movement of dislocations became easier with increases in the austenising and deformation temperatures, and hence the resistance of the material to deformation decreased. Meanwhile, at lower austenising and deformation temperatures, the mobility of the dislocations decreased owing to the increased dislocation density and degree of dislocation tangling, which enhanced the resistance to plastic deformation.

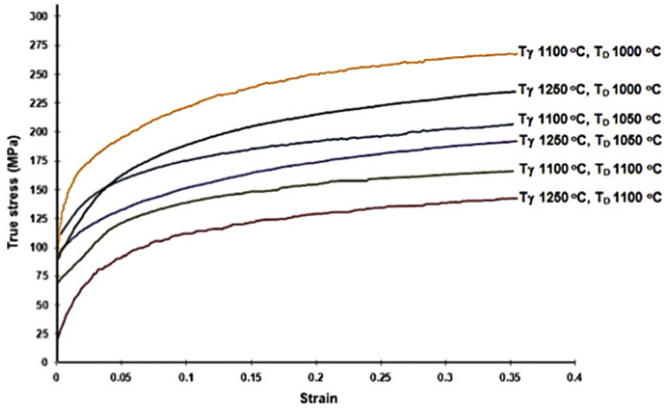

Fig. 5. Flow curves of the H21 tool steel after deformation at 1000, 1050 and 1100 °C with different austenising temperatures (T_D is deformation temperature).

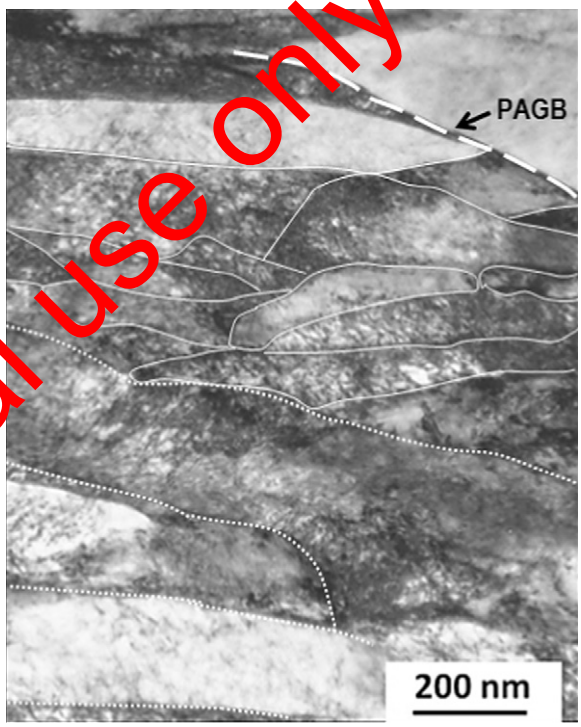

Fig. 6. Bright field TEM image after austenising at 1100 °C and deformation at 1100 °C showing elongated subgrain in the martensite lath. A prior austenite grain boundary (PAGB) is indicated by dashed line, prior martensite laths are indicated by dotted lines and sub-grain boundaries are indicated by full lines.

3.3. The effect of austenising and hot deformation temperatures

It is well known that the microstructure of a material strongly affects its flow behaviour during deformation. The applied low strain rate and hot deformation would provide longer time for energy accumulation and higher mobility of boundaries for the nucleation and growth of dynamically recrystallised grains and dislocation annihilation. However, the microstructure and behaviour of the flow curves showed no evidence that dynamic recrystallisation (DRX) had occurred. Fig. 6 is a bright field TEM image showing the elongated subgrain structures that were present in the lath martensite, typical for dynamic recovery. During hot deformation, the formation of subgrains due to dislocation annihilation and rearrangement decreased rapidly the energy stored in the steel [21].

In this study, there were two dominant factors affecting the absence of DRX in the H21 tool steel, which had high content of

carbide forming elements that produced a significant volume fraction of carbides in the as cast condition. First, the type and volume fraction of carbides present and second, the presence of dispersed carbides after hot deformation. According to Karagoz and Fischmeister [22], the rate of carbide dissolution during austenisation increases in the sequence MC, M_6C, M_7C_3 and $M_{23}C_6$. The MC and M_6C carbides are thermodynamically stable carbides and do not completely dissolve even at high austenising temperature [23]. After austenising for 10 min, undissolved MC and M_6C carbides still existed in the material that was subjected to hot deformation. The undissolved carbides shown in Fig. 7 were M_6C and were confirmed by back scatter imaging. The fine MC carbides were observed by TEM (see below). These undissolved carbides are believed to play an important role in retarding the recrystallisation owing to their presence before any recrystallisation could occur [21], and cause a Zener pinning effect. The grain boundaries were pinned by the carbides, subsequently suppressing any dynamic recrystallisation and stabilised the deformed or recovered microstructure. Carbide precipitates have an important role as pinning agents keeping grain boundaries in place [24,25]. Milovic et al. [26] reported that carbide precipitation retarded the dislocation movement and also the movement of subgrains and grain boundaries, thus suppressing dynamic recrystallisation. The Zener pinning effect became stronger when the volume fraction of these carbides was higher. The higher the austenising and deformation temperatures, the more the carbides were dissolved into the matrix, and as a result, the Zener pinning effect was decreased, as demonstrated by the decreasing flow stress as shown in Fig. 5.

Fig. 7 also shows that the morphology of the carbides in all experimental conditions of this study was almost the same as that of the as-cast structure. The broken carbides were distributed everywhere, not only along the grain boundaries, but also in the grain interiors. The deformation temperature influenced the carbide network in the direction perpendicular to the compression axis and reduced the carbide size effectively. It was noted that at the lower austenising and deformation temperatures, the undissolved carbides were more refined and uniformly dispersed and closely spaced. In general, after hot deformation the average carbide size was less than 1 μm. Dispersed precipitates after hot deformation are known to promote the retardation of recrystallisation. With a sufficiently small spacing of thermodynamically stable precipitates, it is possible to keep the deformed or recovered microstructure up to high temperatures, and subsequently increase the retention of the dislocation substructure at high deformation temperatures, thus providing a strengthening mechanism in addition to that of the precipitates [21]. In this work, the most dispersed and finest of M_6C carbides with average carbide size of ~0.2 μm were observed after austenising at 1100 °C followed by hot deformation at 1000 °C. This is consistent with the flow curves that show that the highest flow stress was obtained after austenising at 1100 °C and deformation at 1000 °C. No cracks were observed in all the deformed specimens.

TEM analysis was carried out to characterise the microstructures. Fig. 8 shows that the microstructure of the tool steel following hot deformation and water quenching consisted of martensite and carbides. The morphology of martensite was of lath type, which is consistent with previous investigations on steels with carbon contents less than 0.4 wt%, and was heavily dislocated [27–29]. The width of martensite laths varied between 0.1 and 0.4 μm, and they were slightly parallel to each other. The morphology of martensite did not change significantly at all the deformation and austenising temperatures; however, the width of the laths was slightly smaller at higher austenising temperatures due to the larger driving force, producing finer martensite laths with a corresponding increase in the hardness. Fig. 8 also shows qualitatively that the higher the austenising and deformation temperatures, the more the free dislocation areas, which indicated lower dislocation density.

The presence of MC carbides that play an important role in retarding the recrystallisation in the as quenched microstructure was confirmed using bright field TEM and SAD (see Fig. 9). The fine spherical MC carbides with size 5–10 nm were observed in the lath martensite. The morphology and size of the MC carbides remained unchanged compared with the as cast condition.

Fig. 10 shows micro-twins appearing in the lath martensite with an average spacing of around 20 nm. To analyse the formation of micro-twins, an additional experiment was performed in which the H21 tool steel was austenised at 1250 °C (without deformation) and then water quenched. TEM analysis of the as quenched sample without deformation found very fine micro-twins in the microstructure, Fig. 11. The formation of micro-twins

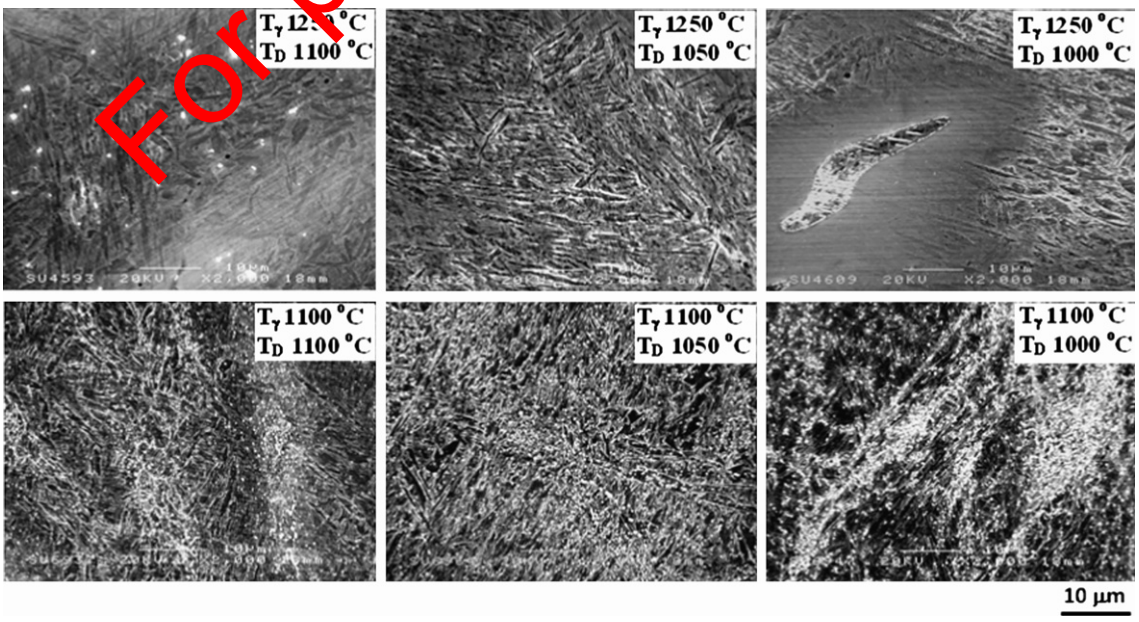

Fig. 7. Secondary electron SEM images of the H21 tool steel after hot deformation and water quenching.

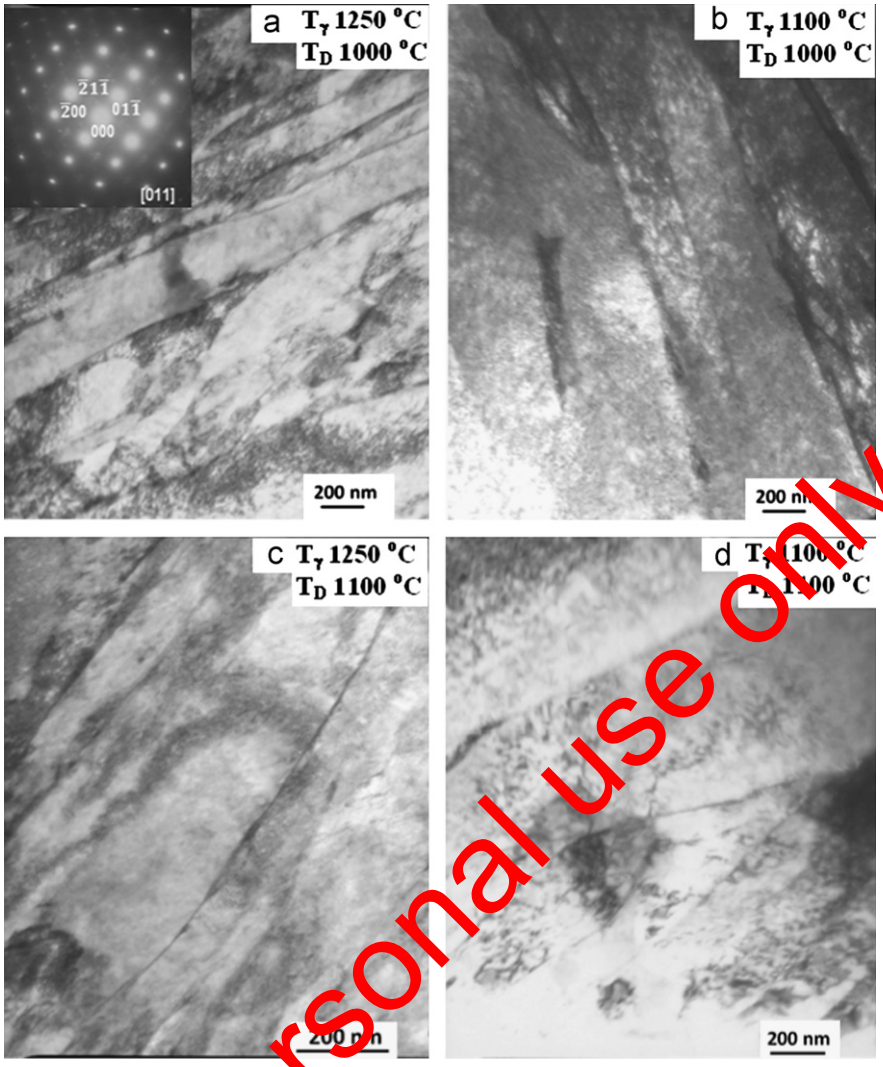

Fig. 8. Bright field TEM images after austenising and deformation. The inset of (a) shows selected area diffraction pattern of martensite region.

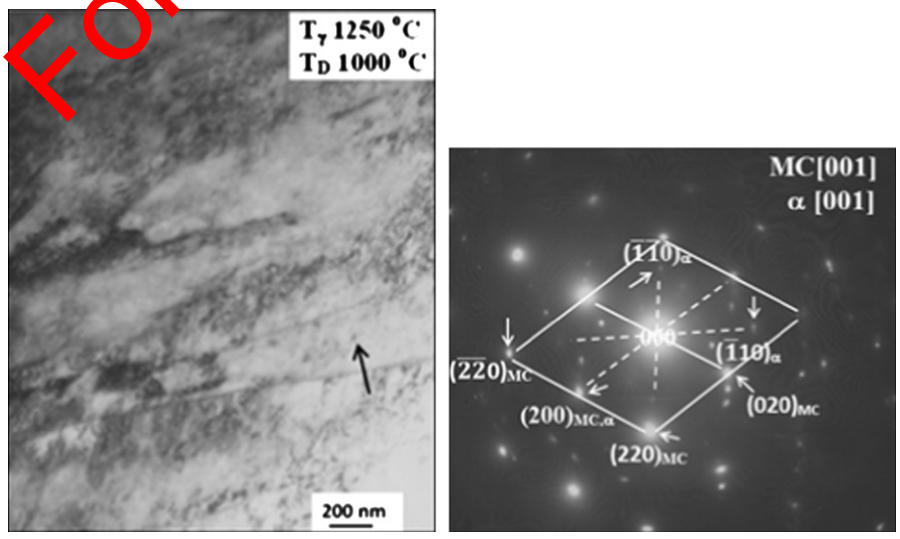

Fig. 9. Bright field TEM image of a martensitic lath showing the MC carbides in the deformed H21 tool steel as indicated by arrow (left) and diffraction pattern of the MC carbide (right).

Fig. 10. Bright field TEM image after austenising at 1250 °C and deformation at 1000 °C showing microtwins.

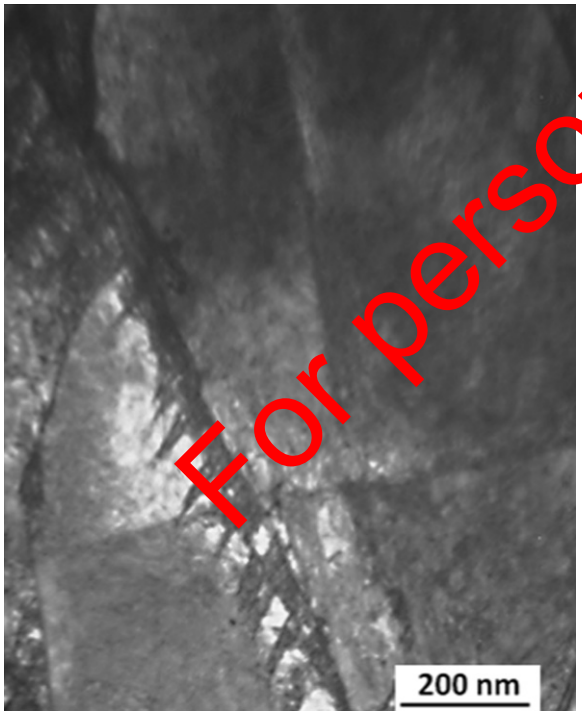

Fig. 11. Bright field TEM image after austenising at 1250 °C and water quenching (without deformation) showing microtwins.

can be explained as follows. During austenisation, the carbides were dissolved into the matrix producing a local area of austenite enriched with carbon. When the rapid cooling was performed, this carbon was trapped in the retained austenite and this retained austenite, rich in carbon, transformed to martensite with micro-twin formation. This formation of micro-twins is more affected by rapid cooling than by the deformation process itself.

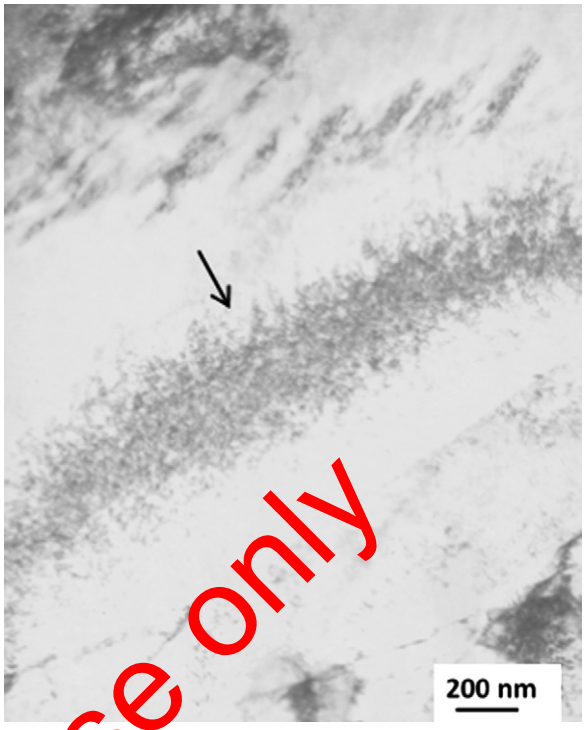

Fig. 12. Bright field TEM image after austenising at 1250 °C and deformation at 1000 °C showing the presence of lower bainite (arrow indicates curved surface).

TEM analysis has also confirmed that lower bainite was present after deformation at 1000 °C and water quenching. A bainite plate with a curved surface can be seen in Fig. 12, due to deformation-induced lattice curvature present in the former austenite grains prior to transformation [30].

Xiao et al. [31] suggested that the presence of undissolved carbides can affect the bainite transformation. Undissolved carbides enable the composition of the austenite to be inhomogeneous during deformation and retard dislocation movement, producing a higher density of dislocations near the carbide. As a consequence of the increased dislocation density and high diffusivity paths, the carbides can dissolve, the carbon concentration becomes higher, producing localised carbon segregation in the hot deformed austenite that subsequently promotes cementite carbide precipitation during the bainite transformation, producing the area with decreasing carbon concentration, which stimulates the nucleation of bainite. In this study, (i) as the deformation temperature decreased, the volume fraction of undissolved carbides increased and the bainite transformation was more pronounced and (ii) the SEM–EDS data shown in Fig. 13 would suggest that the carbon content near the undissolved carbide was slightly higher than that of the martensite area far away from the carbides. These observations could explain why the undissolved carbides influenced the bainitic transformation. However, internal stresses during the transformation from austenite to martensite can also accelerate the formation of bainite [32] as well as the stress applied during hot deformation that produces a high density of dislocations that can affect the bainite transformation by increasing the driving force and transformation kinetics, and reducing the incubation period [33,34].

TEM investigation also found the presence of retained austenite using the dark field technique. Fig. 14 shows the banded morphology of retained austenite in the H21 tool steel after hot deformation and water quenching.

The banded morphology of the retained austenite seems to further indicate that no recrystallisation had occurred during the

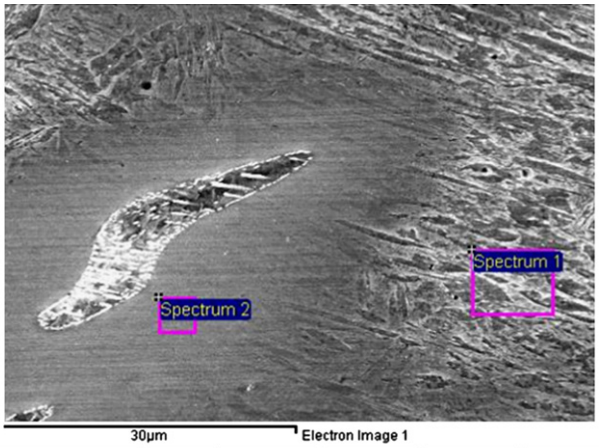

Element (wt%)	C	V	Cr	Fe	W
Spectrum 1	1.76	0.59	3.09	90.18	4.38
Spectrum 2	1.89	0.55	3.23	87.73	6.48

Fig. 13. EDS data of the H21 tool steel after austenising at 1250 °C and deformation at 1000 °C.

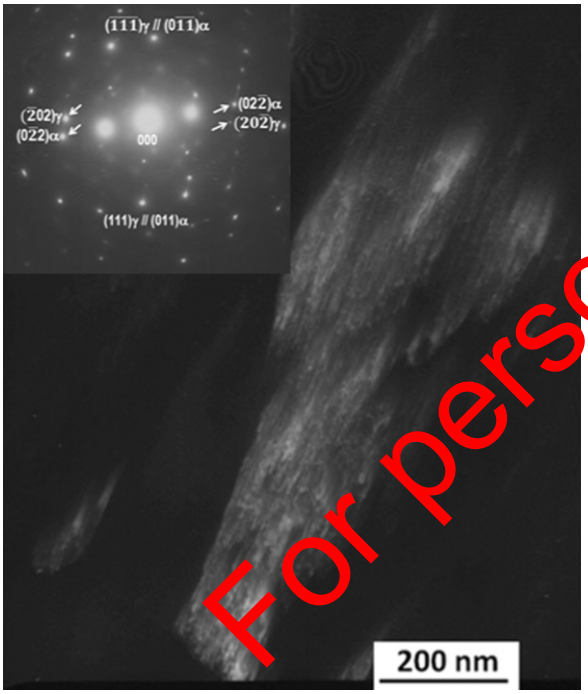

Fig. 14. Dark field TEM image showing retained austenite (T_γ=1100 °C, T_D=1000 °C). The inset shows the selected area diffraction pattern taken at the interface between retained austenite and martensite with $[0\bar{1}1]\gamma // [1\bar{1}1]\alpha$.

time interval following deformation to the start of the transformation. The diffraction pattern in Fig. 14 shows that the orientation of the phases between martensite and austenite was in good agreement with the Kurdjumov–Sachs relation [35]. Although quantitative measurements of the volume fraction of retained austenite were not made, a qualitative assessment indicated that a larger volume fraction of retained austenite was associated with a higher austenising and deformation temperature as a result of more carbides being put into solution, and thus, the C content in austenite was getting higher. The stability of retained austenite is considered to be related to the C content in the austenite phase and the higher the C content, the more stable the retained austenite.

3.4. The effect of double tempering on the microstructure

Due to the high alloying content, it is strongly recommended to temper the hardened tool steel at least twice to improve the toughness and thermal stability of the microstructure which would not be achieved by a single tempering process [1]. The double tempering process also increases the secondary hardness as reported in other investigations [36,37]. A TEM investigation was carried out to support the microstructure analysis. The resulting microstructure consisted of tempered lower bainite, and tempered martensite, with precipitates located along the grain boundaries and within the lath boundaries.

TEM images of the H21 tool steel after isothermal double tempering for 1 h at 650 °C with air cooling in between the first and second stages in Fig. 15 show that the lath morphology was still present and the cementite precipitates can be seen clearly. Needle-shaped cementite precipitates were located within lath and lath boundary and the dislocations were prone to form networks by recovery especially along the grain boundaries. The appearance of cementite precipitates within laths and lath boundary indicated that cementite precipitation occurred in the early stages of tempering. The cementite grew by increasing the tempering temperature [38–40]. The microstructures in Fig. 15 also show that the dislocations formed networks through a recovery process. The latter was not completed as indicated by free dislocations inside a prior martensite lath. The partial recovery was probably due to insufficient time being available for completing the recovery process. The recovery seemed to be more effective at a higher austenising temperature (Fig. 14b and d) and a higher deformation temperature (Fig. 14c and d). This was attributed to the lower dislocation density at the higher austenising and deformation temperatures.

In this study it is believed that no retained austenite remained in all double tempered conditions. During the first tempering, retained austenite transforms to lower bainite in the temperature range 230–300 °C [23,41] and the stability of retained austenite decreases with increasing tempering temperature.

Fig. 15b shows the formation of tempered lower bainite. The major difference between tempered martensite and tempered lower bainite is that the cementite precipitates in lower bainite occur frequently on one crystallographic variant of the orientation relationship. The major axis of the cementite forms parallel arrays at about 60° to the axis of the bainitic lath whereas, in tempered martensite, the carbides tend to precipitate in the Widmanstätten arrays. The occurrence of single variants in lower bainite as illustrated in Fig. 15b is due to the small driving force for cementite precipitation where carbon can diffuse very fast away from the supersaturated ferrite [42].

The TEM images presented in Fig. 16 show the H21 tool steel after isothermal double tempering at 800 °C with air cooling in between the first and second stages, and illustrate that the lath morphology had disappeared and equiaxed grains tended to form with clear boundaries and larger carbides. The TEM images in Fig. 16 also show clearly that the carbides located along the grain boundaries were larger than those within the grain interiors which would suggest that the stable carbides nucleated first in the grain boundaries and grew rapidly and replaced non-stable carbides within the grains. In summary, the growth rate of the carbides was faster at the grain boundaries [43]. The formation of alloy carbides to replace cementite carbides occurred by nucleation at prior austenite grain boundaries that are energetically favourable nucleation sites [44]. At the higher austenising

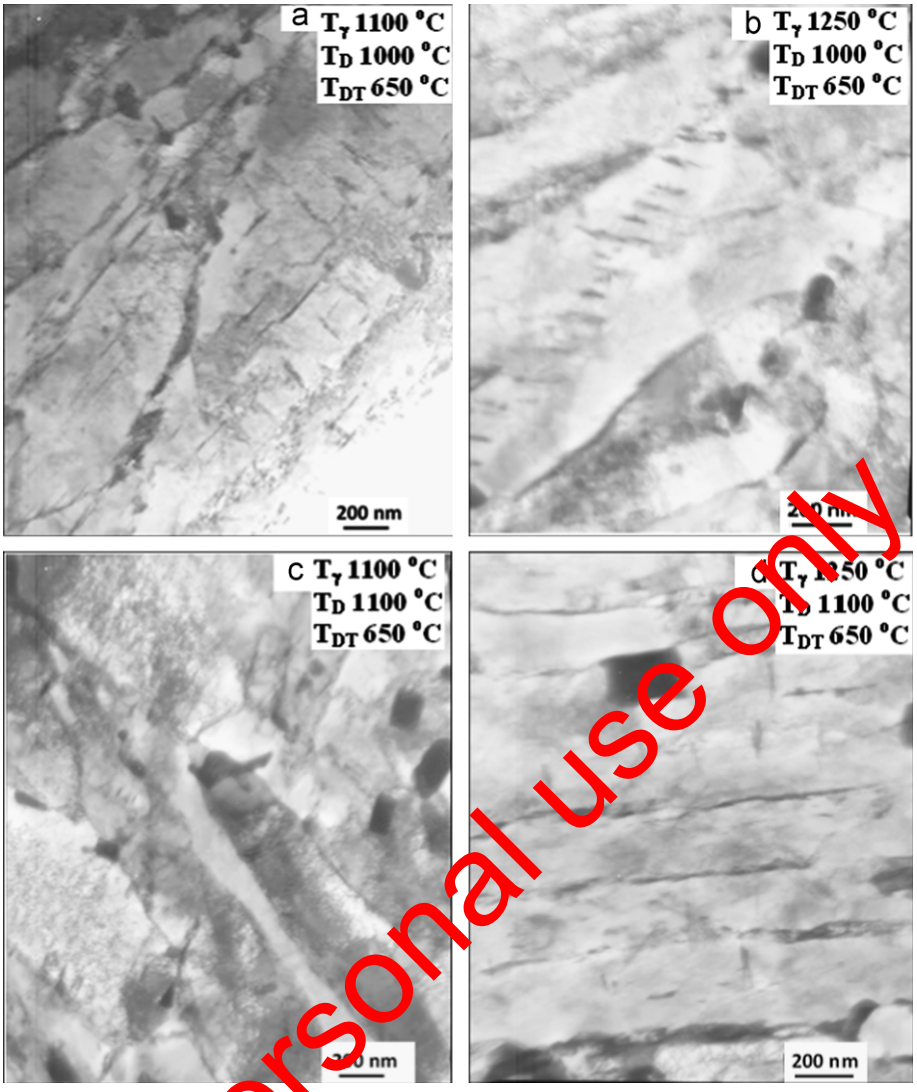

Fig. 15. Bright field TEM images after austenising, hot deformation and double tempering showing the formation of tempered lath martensite (a, c and d) and tempered lower bainite (b).

temperatures, the cementite carbides became slightly coarser. The thickness of cementite carbides was finer at the lower austenising and lower hot deformation temperatures, but the refinement of cementite carbides was not clear when tempering at 800 °C due to the presence of secondary carbides that coarsened rapidly.

3.5. The hardness behaviour

The austenising temperatures affected the hardness of the steel in the as-quenched and double tempered condition (Table 2).

The higher austenising temperature with and without deformation gave higher hardness than that of the lower austenising temperature. The highest hardness with deformation (617 HV) of the H21 tool steel occurred after austenising at 1250 °C, followed by deformation at 1000 °C. The highest hardness without deformation (574 HV) occurred after austenising at 1250 °C. This was attributed to a higher volume fraction of carbides dissolved into the matrix at higher austenising temperatures, thus enriching the matrix with alloying elements. The hardness increased with decreasing deformation temperatures at both austenising temperatures, owing to the higher volume fraction of dispersed carbides that existed at lower deformation temperatures.

The temperature at which double tempering took place also affected the hardness of the tool steel. Table 3 shows the hardness variation as a function of tempering temperature.

The double tempered hardness after hot deformation decreased significantly and was lower than the hardness after double tempering without deformation (505 HV), and the double tempered hardness decreased continuously with increasing tempering temperature at both austenising temperatures. However, the double tempered hardness after austenising at 1250 °C was higher than that at 1100 °C. As explained before, this is because at higher austenising temperatures, more carbides were dissolved into the matrix, giving a higher super saturation and driving force for precipitation, which in turn provided more nucleation sites for carbide precipitation during the double tempering process.

The highest double tempered hardness (354 HV) occurred after double tempering at 650 °C with austenising temperature of 1250 °C and deformation temperature of 1000 °C. The values are lower and far from the desired hardness, which is 450–550 HV [1]. This implies that the operating temperature for the H21 tool steel after experiencing hot deformation should be less than 650 °C. Softening of hot work tool steels during tempering

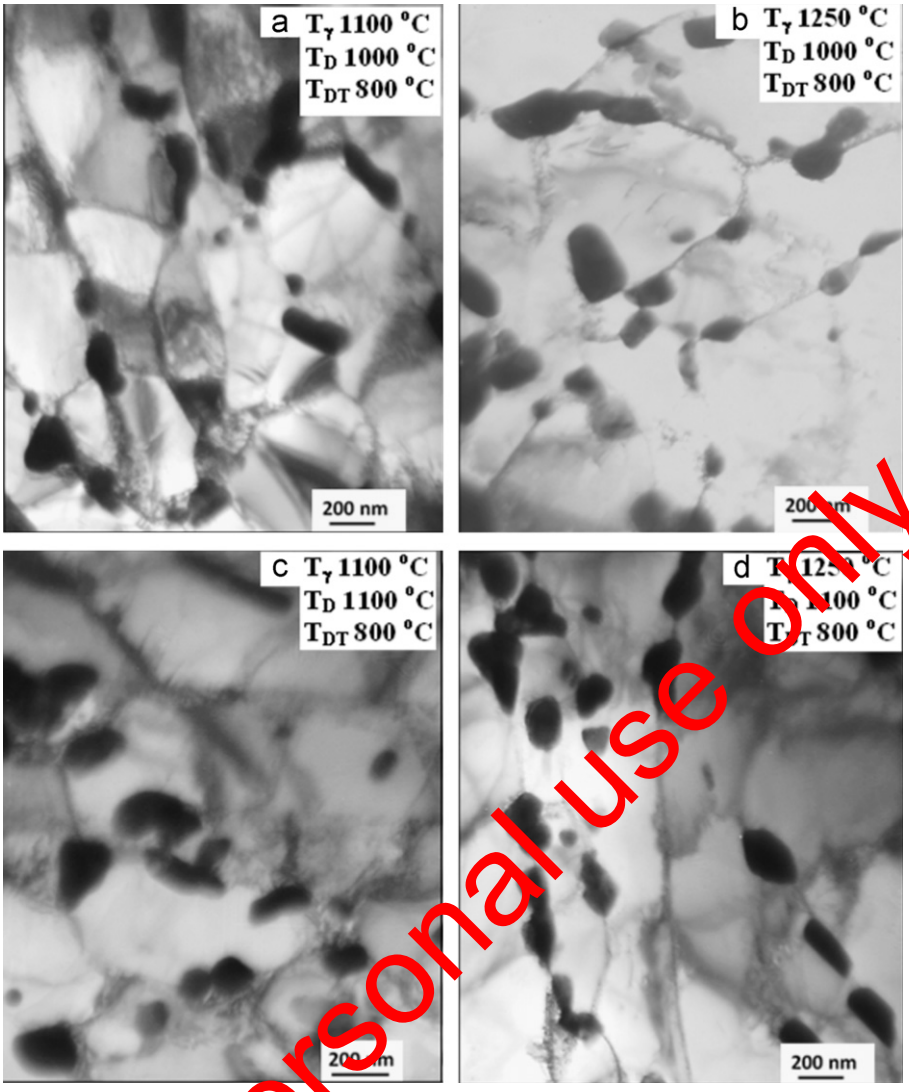

Fig. 16. Bright field TEM images after austenising, hot deformation and double tempering.

Table 2
Effect of hot deformation on hardness.

Austenising temperature (°C)	Hardness (HV)			
	Hot deformation and water quenching			Water quenching (without deformation)
	Deformation temperature (°C)			
	1000	1050	1100	
1250	617 ± 4	589 ± 1	569 ± 1	574 ± 1
1100	570 ± 4	535 ± 3	524 ± 2	536 ± 7

has been strongly connected with the evolution of carbide precipitation and martensite decomposition. Deformation affected the tempering resistance of the tool steel resulting in rapid softening as the deformation temperature increased. The deformation accelerated the sequence of carbide precipitation in which the fine carbides (M_2C) that are responsible for secondary hardening were gradually replaced by coarse cementite carbides during tempering at 650 °C [45]. The acceleration of carbide precipitation was due to an increased vacancy concentration by the deformation and the local residual strain which created more opportunities for carbide nucleation and greater mobility of carbide forming elements [46]. Higher tempering temperatures resulted in a decrease in hardness due to coarsening of carbide precipitates and the recovery of the dislocation-rich martensitic structure and ferrite grain growth. No secondary hardening occurred. This implies that in the tool steel of this study, the secondary hardening during double tempering after hot deformation occurs below 650 °C.

4. Conclusions

The primary carbides observed in the as cast H21 tool steel were predominantly of M_6C type, which were tungsten-rich exhibiting an fcc crystal structure, and MC type carbides. The hot deformation process showed that no dynamic recrystallisation occurred for all processing parameters. The as quenched microstructure after hot deformation consisted of lath martensite, lower bainite, retained austenite and carbides. The relationship between the product martensite and parent austenite was in good agreement with the Kurdjumov–Sachs orientation.

The flow stress, microstructure and hardness data indicated that the optimum hot deformation condition was after austenising at 1250 °C and subsequent deformation at 1100 °C. After hot

Table 3
Effect of double temper on hardness.

Hot deformation				Without deformation		
T_γ (°C)	Deformation temperature (°C)	Double tempering temperature (°C)	Hardness (HV)	T_γ (°C)	Double tempering temperature (°C)	Hardness (HV)
1100	1000	650	311 ± 2.4	1100	650	422 ± 1.8
		750	244 ± 2.2			
		800	237 ± 2.1			
	1050	650	306 ± 2.0		750	247 ± 1.2
		750	235 ± 1.2			
		800	232 ± 0.7			
	1100	650	303 ± 1.2		800	236 ± 0.8
		750	234 ± 1.4			
		800	231 ± 1.6			
1250	1000	650	354 ± 2.4	1250	650	505 ± 1.0
		750	264 ± 2.0			
		800	237 ± 3.3			
	1050	650	347 ± 2.3		750	270 ± 1.1
		750	260 ± 0.8			
		800	234 ± 2.0			
	1100	650	336 ± 2.1		800	247 ± 1.1
		750	256 ± 2.2			
		800	233 ± 1.7			

deformation and double tempering, the microstructure of the investigated tool steel consisted of tempered martensite, tempered lower bainite and carbides. No secondary hardening phenomenon occurred after double tempering at 650, 750 and 800 °C for samples that were first subjected to hot deformation. It is concluded that the operating temperature for the H21 tool steel after experiencing hot deformation with the conditions used in this study should be less than 650 °C.

Acknowledgements

The author (MN) would like to thank the Directorate General of Higher Education, Indonesian Government and the Institut Teknologi Nasional, Bandung for their financial support.

References

[1] G.A. Roberts, G. Krauss, R.L. Kennedy (Eds.), Tool Steels, fifth ed.,ASM International, Metals Park, Ohio, 1998.
[2] R.M. Brick, A.W. Pense, R.B. Gordon, Structure and Properties of Engineering Materials, fourth ed., Mc-Graw–Hill Book Company, New York, 1977.
[3] M. Pavlı´čková, D. Vojtěcha, P. Novák, J. Gemperlová, A. Gemperleb, N. Zárubová, P. Lejček, P. Jurč, P. Šolar, Mater. Sci. Eng. A 356 (2003) 200–207.
[4] C.A.C. Imbert, N.D. Ryan, H.J. McQueen, Metall. Mater. Trans. A 15A (1984) 1855–1864.
[5] M.R. Ghomashchi, C.M. Sellars, Metall. Mater. Trans. A 24A (1993) 2171–2180.
[6] D. Jandova, J. Rehor, Z. Novy, J. Mater. Process. Technol. 157–158 (2004) 523–530.
[7] E.S. Lee, W.J. Park, K.H. Baik, S. Ahn, Scr. Mater. 39 (1998) 1133–1138.
[8] N. Isasti, D. Jorge-Badiola, M.L. Taheri, B. López, P. Uranga, Metall. Mater. Trans. A 42 (2011) 3729–3742.
[9] Y. Van-Leeuwen, J. Sietsma, Mater. Sci. Forum 539-543 (2007) 4572–4577.
[10] D.N. Hanlon, J. Sietsma, S.V.D. Zwaag, ISIJ Int. 41 (2001) 1028–1036.
[11] C.A.C. Imbert, H.J. McQueen, Mater. Sci. Eng. A 313 (2001) 88–103.
[12] W. Roberts, in: A.G. Krauss (Ed.), Processing and Structure, ASM International, Metals Park, Ohio, 1982, pp. 109–184.
[13] C.A.C. Imbert, H.J. McQueen, Mater. Sci. Technol. 16 (2000) 524–531.
[14] C.A.C. Imbert, H.J. McQueen, Mater. Sci. Eng. A 313 (2001) 104–116.
[15] T.V. Pirtovšek, G. Kugler, M. Godec, M. Terčelj, Mater. Charact. 62 (2011) 1–9.
[16] N.D. Ryan, H.J. McQueen, J. Mech. Work. Technol. 12 (1986) 323–349.
[17] L.A. Dobrzański, J. Mater. Process. Technol. 38 (1993) 123–134.
[18] P. Fajfar, D. Bombač, I. Markoli, RMZ Mater. Geoenviron. 57 (2010) 159–164.
[19] H. Conrad, S. Feuerstack, Acta Metall. 10 (1962) 1013–1020.
[20] W.-S. Lee, C.-Y. Liu, Mater. Sci. Eng. A 426 (2006) 101–113.
[21] F.J. Humphreys, M. Hatherly, Recrystallization and Related Annealing Phenomena, first ed., Elsevier Science Ltd., Oxford, 2004.
[22] S. Kirkaldy, H. Fischmeister, Steel Res. 58 (1987) 353–361.
[23] G.E. Totten, Steel Heat Treatment: Metallurgy and Technologies, second ed., Taylor and Francis, New York, 2006.
[24] A. Kostka, K.G. Tak, R.J. Hellmig, Y. Estrin, G. Eggeler, Acta Mater. 55 (2007) 539–590.
[25] A. Momeni, K. Dehghani, H. Keshmiri, G.R. Ebrahimi, Mater. Sci. Eng. A 527 (2010) 1605–1611.
[26] R. Milovic, D. Manojlovic, M. Andjelic, D. Drobnjak, Steel Res. 63 (1992) 78–84.
[27] E.A. Wilson, ISIJ Int. 34 (1994) 615.
[28] A.R. Marder, G. Krauss, Trans. Am. Soc. Met. 60 (1967) 651–660.
[29] D.A. Mirzayev, V.M. Schastlivtsev, S.Y. Karzwnov, Fiz. Met. Metalloved. 63 (1987) 764.
[30] H.K.D.H. Bhadeshia, Bainite in Steels: Transformation, Microstructures and Properties, second ed., The Institute of Materials Communication Ltd, 2001.
[31] F. Xiao, B. Liao, G. Qiao, S. Guan, Mater. Charact. 57 (2006) 306–313.
[32] S.V. Radcliffe, E.C. Rollason, J. Iron Steel Inst. 191 (1959) 56–65.
[33] K. Hase, C. Garcia-Mateo, H.K.D.H. Bhadeshia, Mater. Sci. Technol. 20 (2004) 1499–1505.
[34] P.H. Shipway, H.K.D.H. Bhadeshia, Mater. Sci. Eng. A 201 (1995) 143–149.
[35] R.E. Smallman, A.H.W. Nagan, Physical Metallurgy and Advance Materials, seventh ed., Elsevier Ltd., 2007.
[36] M.L. Fares, M. Athmani, Y. Khelfaoui, A. Khettache, Mater. Sci. Eng. 28 (2012) 1–10.
[37] J. Hufenbach, L. Giebeler, M. Hoffmann, S. Kohlar, U. Kühn, T. Gemming, S. Oswald, B. Eigenmann, J. Eckert, Acta Mater. 60 (2012) 4468–4476.
[38] G.R. Speich, Trans. Metall. Soc. AIME 245 (1969) 2553–2564.
[39] V.Z.B. Hernandez, S.S. Nayak, Y. Zhou, Metall. Mater. Trans. A 42 (2011) 3115–3129.
[40] F.G. Caballero, M.K. Miller, S.S. Babu, C. Garcia-Mateo, Acta Mater. 55 (2007) 381–390.
[41] H.K.D.H. Bhadeshia, R.W.K. Honeycombe, Steels Microstructure and Properties, third ed., Elsevier Ltd., Oxford, 2006.
[42] H.K.D.H. Bhadeshia, Acta Metall. 28 (1980) 1103–1114.
[43] M.V. Speight, Acta Metall. 16 (1968) 133–135.
[44] M. Durrand-Charre, Microstructure of Steels and Cast Irons, Springer-Verlag, Berlin, 2004.
[45] J.S. Lee, J.S. Chun, Mater. Sci. 16 (1981) 1557–1566.
[46] E.C. Bain, H.W. Paxton, Alloying Elements in Steels, second ed., ASM International, Metals Park, Ohio, 1966.